Home   Search   Collections   Journals   About   Contact us   My IOPscience

Ferromagnetic resonance with long Josephson junction

Ferromagnetic resonance with long Josephson junction

I A Golovchanskiy[1,2]**, N N Abramov**[2]**, V S Stolyarov**[1,3,4]**, O V Emelyanova**[5]**, A A Golubov**[1,6]**, A V Ustinov**[2,7,8] **and V V Ryazanov**[2,3,4,9]

[1] Moscow Institute of Physics and Technology, State University, 9 Institutskiy per., Dolgoprudny, Moscow Region, 141700, Russia

[2] National University of Science and Technology MISIS, 4 Leninsky prosp., Moscow, 119049, Russia

[3] Institute of Solid State Physics (ISSP RAS), Chernogolovka, 142432, Moscow region, Russia

[4] Solid State Physics Department, Kazan Federal University, 420008 Kazan, Russia

[5] National Research Nuclear University MEPhI, 31 Kashirskoye sh., 115409 Moscow, Russia

[6] Faculty of Science and Technology and MESA+ Institute for Nanotechnology, University of Twente, 7500 AE Enschede, The Netherlands

[7] Physikalisches Institut, Karlsruhe Institute of Technology, D-76131 Karlsruhe, Germany

[8] Russian Quantum Center, Novaya str. 100, BC Ural, Skolkovo, Moscow region, 143025, Russia

E-mail: ryazanov@issp.ac.ru

CrossMark

Abstract

In this work we propose a hybrid device based on a long Josephson junction (JJ) coupled inductively to an external ferromagnetic (FM) layer. The long JJ in a zero-field operation mode induces a localized AC magnetic field in the FM layer and enables a synchronized magnetostatic standing wave. The magnetostatic wave induces additional dissipation for soliton propagation in the junction and also enables a phase locking (resonant soliton synchronization) at a frequency of natural ferromagnetic resonance. The later manifests itself as an additional constant voltage step on the current–voltage characteristics at the corresponding voltage. The proposed device allows to study magnetization dynamics of individual micro-scaled FM samples using just DC technique, and also it provides additional phase locking frequency in the junction, determined exclusively by characteristics of the ferromagnet.

(Some figures may appear in colour only in the online journal)

1. Introduction

Josephson tunnel junctions, voltage-tunable oscillators with the Josephson voltage–frequency relation, are employed extensively as the basic element in superconducting classical and quantum electronics. The most widely used are so-called lumped Josephson junctions (JJs). Dimensions of lumped JJs are negligible compared to the Josephson penetration depth λ_J, that allows the consideration of properties of JJs with the integral rather than the local characteristics, including the Josephson phase difference φ or its derivative φ_x, and

the Josephson critical current I_c. Over the last decade there has been a boost of various applications of lumped JJs, including their implementation in SQUIDs [1–3], ultra-fast superconducting electronics [4–9], hybrid Josephson magnetic devices [10–15], superconducting meta-materials [16–19] and quantum bits [20].

A separate class of superconducting devices is based on so-called one-dimensional long Josephson tunnel junctions (LJJ) that are large in one dimension with respect to λ_J, whereas the width is small compared to λ_J. Practical interest in LJJs is attributed to fluxon propagation at applied magnetic field or fluxon (soliton) dynamics at zero field, and to corresponding nonlinear/resonant phenomena of the fluxon

---

[9] Author to whom any correspondence should be addressed.

motion, which can not be depicted with the integral characteristics. The flux-flow (FF) [21–23] operation mode of the LJJ was explored decades ago [24] as a simple mechanism of multi-fluxon propagation in a long one-dimensional JJ. The FF mode is observed at sufficiently high applied magnetic field and can be described briefly as a unidirectional viscous flow of fluxons, created at one end of the junction and annihilated at the other. The JJ operated in the FF mode has attracted considerable attention in view of its applications, e.g., as a local oscillator for integrated submillimeter-wave receivers [25, 26] or nonreciprocal transmitters [27].

Another interesting operation mode of the LJJ appears at zero or small magnetic fields, when the resonant propagation of fluxons as solitons can be observed. The soliton is a 2π kink in the phase difference φ across the insulating barrier, which contains the magnetic flux quantum Φ_0. Moving with a velocity $\bar{v}$ along the junction, the soliton is accompanied by a voltage pulse which can be detected at either boundary of the junction, as well as by a magnetic flux pulse. The DC manifestation of the motion is a sequence of equidistantly spaced branches in the current–voltage (I–V) characteristic of the junction. These near-constant voltage branches are known as zero-field steps [28–32] (ZFSs) because they occur in the absence of external magnetic field.

The ZFSs appear at voltages given by $V = N\Phi_0\bar{c}/L$, where N is a number of solitons, $\bar{c} = \lambda_J\omega_J$ is the limiting soliton velocity in the junction (i.e. the Swihart velocity), ω_J is the Josephson plasma frequency, and L is the length of the junction. The soliton arriving at the junction boundary undergoes reflection into the anti-soliton, which is then driven back into the junction by the bias current. On the first ZFS ($N = 1$) a single soliton oscillates back and forth along the straight junction with a velocity $\bar{v} \leqslant \bar{c}$, hence producing a periodic voltage-pulse train of frequency $\bar{v}/L$ and AC magnetic field-pulse train of frequency $f_J = \bar{v}/2L \leqslant f_{ZFS} = \bar{c}/2L$. On the Nth ZFS the motion of N solitons is involved and N pulses are produced within one period $1/f_J$.

Importantly, the LJJ in a dynamic mode can couple effectively to the external environment. The coupling is reflected by the corresponding features on I–V characteristics. Resonant coupling effects are referred commonly as phase-locking or soliton synchronization. Coupling of fluxons to the external microwave field results in Shapiro-like steps on I–V characteristics at the corresponding voltage in both zero-field [33–36] and FF operation modes [27]. Intrinsic phase locking between coupled LJJs also takes place in both the FF mode [37, 38] and the ZFS mode [39, 40], and is induced by inductive coupling of vortex currents circulating in the shared superconducting electrode layer. The most important for this work is a responsiveness of soliton dynamics in the LJJ to *nonuniform* external magnetic field, which was studied employing circular LJJs. Uniform DC magnetic field enables pinning of a soliton in circular LJJ [41–43], while RF magnetic field forces soliton synchronization [44, 45]. The most spectacular is synchronization of the soliton in circular LJJ with external rotating magnetic field [46]. Therefore, once the external nonuniform magnetic field appears, the corresponding response on ZFS I–V characteristic is expected.

In this work, we explore the following hybrid device based on a LJJ coupled to a ferromagnetic (FM) layer. We consider a straight LJJ in the ZFS operation mode. A shuttling soliton generates a small AC magnetic field of frequency f_J in the middle of the LJJ. The AC soliton field can be absorbed by the FM layer placed in close proximity to the LJJ, inducing a spatially nonuniform precession of its magnetization, according to Landau–Lifshitz–Gilbert dynamics. The non-uniform precession enables a corresponding spatially non-uniform periodic magneto-static field in the LJJ and should affect the dynamics of the soliton. This effect should be notable on I–V characteristics. If f_J matches the ferromagnetic resonance (FMR) frequency (f_{FMR}), a step-like feature is expected on the ZFS I–V characteristics, manifesting synchronization of fluxon motion in the LJJ with the FM. Since the ZFS Josephson frequency $f_J \sim 1/L$, it can be simply adjusted to f_{FMR} varying the length of the device.

Magnetization precession and its resonance (i.e. FMR) are fundamental phenomena of a FM material. FMR at zero magnetic field is referred commonly as natural FMR. The frequency of the natural FMR is justified by the saturation magnetization and effective magnetic anisotropy of extrinsic (shape anisotropy) or intrinsic (magneto-crystalline anisotropy) origin, according to the Kittel formulas [47, 48]. One may note that natural f_{FMR} of conventional FM materials does not exceed several GHz. At the same time, Swihart velocity of a typical high-quality superconductor-insulator-superconductor (SIS) junctions is $\bar{c} \sim 10^6 - 10^7$ m s^{-1} providing a limiting f_J frequency in the range of $(0.1 - 1) \times 10^3$ GHz for a length of several tens of μm [49–55]. Such frequency mismatch makes synchronization of SIS LJJ with a conventional FM unfeasible. Nevertheless, several classes of FMc materials exist with exceptional magnetic anisotropy and corresponding high natural f_{FMR}. On the other hand, in general, the Swihart velocity in SIS can also be reduced by appropriate selection of the tunnel barrier (its thickness and permittivity), as well as by employing superconducting electrodes with larger London penetration depth. In this work, we consider the hybrid device aiming realistic FM and SIS properties.

This work is organized as follows. In section 2 we describe the proposed hybrid device and provide its detailed self-consistent numerical model. In section 3.1 we discuss the synchronization of the soliton motion in high quality Nb/AlO$_x$/Nb LJJ to magnetization dynamics in FePt FM layer with strong out-of-plane magnetic anisotropy. In section 3.2 we demonstrate the synchronization of the soliton motion in MgB$_2$/AlN/NbN LJJ with low Swihart velocity to magnetization dynamics in CoFeB FM layer with high in-plane magnetic anisotropy. The work is summarized in section 4.

2. Description of the hybrid device

Figure 1 shows a schematic illustration of the proposed hybrid device of the length L. Two superconducting electrodes (S) are separated by the insulating (I) tunnel barrier of the width W (shown in black) and the FM layer of the same width
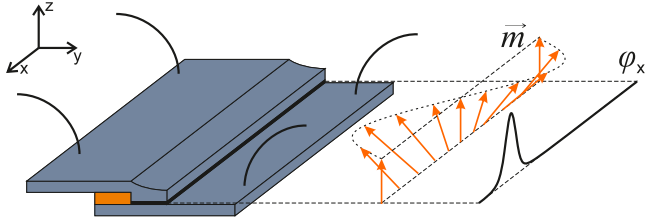
Figure 1. A schematic illustration of the hybrid device. Ferromagnetic layer (shown in orange) is placed in close proximity to the insulating Josephson tunnel layer (shown in black). Black solid curve denotes the magnetic flux produced by the soliton (i.e. a phase gradient φ_x). Orange arrows denote local magnetization orientation ($\vec{m}$) appeared due to engagement with AC magnetic field of soliton. $\vec{m}$ and φ_x are coupled inductively. The case when magnetization is saturated along out-of-plane (z) easy magnetization axis is illustrated.

(shown in orange). The I layer and the FM layer can be fabricated in contact. The magnetization of the FM sample is saturated along the easy magnetization axis aligned either in-plane, in x-direction, or out-of-plane, in z-direction. The device with the out-of-plane easy magnetization axis of the FM layer is depicted in figure 1. Since the FM layer has large thickness d_F, superconducting current flows through the SIS junction only (i.e. no proximity effect through the FM exists). However, S electrodes provide screening for both the magnetic field produced by the soliton as well as for FM magnetostatic field. Therefore, within the proposed design the entire magnetic flux produced by the soliton will penetrate the FM, while y-component of magnetostatic field of the FM penetrates the SIS. Unwanted out-of-plane magnetostatic field in the LJJ induced by the FM with out-of-plane magnetization can be compensated by out-of-plane applied magnetic field.

Dynamics of the LJJ of the length L is described comprehensively by one-dimensional perturbed sine-Gordon equation for the Josephson phase difference φ (see for example [56])

$$\beta\varphi_{xxt} + \varphi_{xx} - \varphi_{tt} - \alpha_J\varphi_t - \sin\varphi + \gamma_J - h_x = 0 \quad (1)$$

with corresponding boundary conditions [29, 57, 58]

$$\varphi_x|_{x=0} + \beta\varphi_{xt}|_{x=0} = H^{\text{ext}}|_{x=0}/J_c\lambda_J = -\eta|_{x=0},$$
$$\varphi_x|_{x=L} + \beta\varphi_{xt}|_{x=L} = H^{\text{ext}}|_{x=L}/J_c\lambda_J = -\eta|_{x=L}. \quad (2)$$

In equations (1) and (2) units are normalized by the Josephson penetration depth ($x \to x/\lambda_J$) and by the Josephson plasma frequency ($t \to t\omega_J$), where $\lambda_J = \sqrt{\frac{\Phi_0}{2\pi\mu_0 J_c d_J}}$ and $\omega_J = \sqrt{\frac{2\pi t_{\text{ox}} J_c}{\Phi_0\varepsilon_0\varepsilon}}$, μ_0 is the vacuum permeability, J_c is the critical current density, $d_J = 2\lambda_L + t_{\text{ox}}$ is the magnetic thickness of the junction, t_{ox} is the thickness of the tunnel barrier, λ_L is the London penetration depth, ε_0 is the vacuum permittivity and ε is the permittivity of tunnel barrier. In equation (1), $\beta = \omega_J L_{\text{ind}}/R$ is the surface loss parameter and $\alpha_J = G/\omega_J C$ is the dissipation coefficient, $L_{\text{ind}} = \mu_0 d_J$ is the surface inductance along the LJJ per unit area, R is the surface resistance along the LJJ per unit area, G is the effective shunt quasi-particle conductance across the barrier,

$C = \varepsilon_0\varepsilon/t_{\text{ox}}$ is the specific capacitance of the junction due to the overlap of two superconducting electrodes, $\gamma_J = I_B/I_c = J_B/J_c$ is the normalized bias current uniformly distributed along the LJJ (i.e. a uniform bias feed is considered). Since we consider the zero field mode, the only source of external magnetic field in LJJ is the y-component of magnetostatic field $H^{\text{ext}} = H_y^F$ induced by nonuniform magnetization of FM. The external magnetic field enters the LJJ via boundary conditions in equation (2) as well as via field derivative h_x in equation (1). Validity of equation (1) for description of the long JJ in nonuniform magnetic field was shown experimentally [27, 37, 38, 42, 43, 46, 59]. Soliton currents in LJJ electrodes produce the external magnetic field in FM $H^J = \lambda_J J_c(\beta\varphi_{xt} + \varphi_x)d_J/d_F$.

Dynamics of magnetic moment in the FM layer can be described effectively using micromagnetic simulations. Micromagnetic simulation [60] is based on numerical solution of the Landau–Lifshitz–Gilbert equation for local unit macrospin vectors $\vec{m} = \vec{m}(x, y)$ placed in local reduced effective magnetic fields $\vec{h}_{\text{eff}} = \vec{h}_{\text{eff}}(x, y)$:

$$\frac{d\vec{m}}{dt} = \vec{m} \times \vec{h}_{\text{eff}} + \alpha_F\vec{m} \times \vec{m} \times \vec{h}_{\text{eff}}, \quad (3)$$

where timescale t is unitless and is reduced with $(1 + \alpha_F^2)/(\gamma_0 M_s)$, γ_0 is the gyromagnetic ratio, M_s is the saturation magnetization of a simulated ferromagnet, α_F is the Gilbert damping constant. In equation (3) both $\vec{m}$ and $\vec{h}_{\text{eff}}$ are normalized by M_s. Field $\vec{h}_{\text{eff}}$ typically includes reduced exchange field of local macrospin interaction $\vec{h}_e$, reduced field of magnetostatic interaction $\vec{h}_d$, reduced anisotropy field $\vec{h}_a$ and reduced applied magnetic field $\vec{h}$:

$$\vec{h}_{\text{eff}} = \vec{h} + \vec{h}_e + \vec{h}_a + \vec{h}_d. \quad (4)$$

Since the soliton in the LJJ is the only source of external magnetic field for the FM, $h_y = h^J = H^J/M_s$. Nonuniform magnetization of the FM, induced by the moving soliton, provides the magnetostatic field H_y^F in the LJJ, which enters the sine-Gordon equation (1) via the derivative $h_x = dH_y^F/dx/(\lambda_J J_c)d_F/d_J$ and via the boundary conditions $\eta|_{x=0,L} = -H_y^F|_{x=0,L}/(\lambda_J J_c)d_F/d_J$ (equation (2)).

Therefore, mutual coupling of the LJJ and the FM is realized via magnetostatic field induced by the FM (H_y^F) and via magnetic field of soliton (H^J). These fields are mutually scaled with the d_F/d_J factor and are considered to be uniform along the y- and z-axis (figure 1). The coupled LJJ/FM system is self-consistent. For simulation the entire system of equations (equations (1)–(4)) is solved simultaneously. We employ a Crank–Nicolson numerical scheme for LJJ simulation (equations (1) and (2) and incorporated second-order Runge–Kutta numerical scheme for the FM (equations (3) and (4)). Standard Newman boundary conditions are employed for exchange field $\vec{h}_e$ and standard demagnetizing tensor [61] is employed for $\vec{h}_d$ with fast Fourier transform. At each current step γ_J the system of equations is solved until the convergence is reached for LJJ solution. A leap-frog scheme is used when solutions for LJJ and FM at previous current step are employed as initial conditions at next current step.

It is important to note that a range of typical time scales in JJ $t \sim \omega_J^{-1} \sim 2 \times 10^{-12} - 1 \times 10^{-11}$ s matches the range of typical time scale in FM materials $t \sim (\gamma_0 \times M_s)^{-1} \sim 5 \times 10^{-12} - 3 \times 10^{-11}$ s. This correlation makes coupling of the LJJ with the FM layer and its numerical representation realizable.

3. Results and discussion

3.1. High quality SIS LJJ coupled to the FM with ultra-high out-of-plane anisotropy

First, we wish to consider the hybrid device based on a state-of-the-art Nb/AlO$_x$/Nb SIS JJ [54, 55] with the following properties, attainable at low temperature <1 K: the critical current density $J_c = 4 \times 10^7$ A m^{-2}, the permittivity of AlO$_x$ tunnel barrier $\varepsilon \simeq 10$, the thickness of the barrier $t_{ox} \sim 1$ nm, the London penetration depth $\lambda_L \simeq 5 \times 10^{-8}$ m, the dissipation coefficient $\alpha_J = 0.01$, the surface loss parameter $\beta = 0.002 \ll \alpha_J$. These parameters provide the Josephson penetration depth $\lambda_J \sim 8$ μm, the Josephson frequency $\omega_J \sim 1.12 \times 10^{12}$ Hz and the Swihart velocity $\bar{c} = 10^7$ m s^{-1}. The Swihart velocity determines the limiting AC frequency of soliton field $f_{ZFS} = 250$ GHz for a 20 μm junction [55]. Thus, the FM should have natural f_{FMR} of the order of 100 GHz for synchronization with the soliton.

To our best knowledge, the highest values of magneto-crystalline anisotropy and of corresponding natural f_{FMR} are observed in chemically ordered thin films with out-of-plane anisotropy. In particular, chemically ordered equiatomic FePt thin films with $L1_0$ crystal structure exhibit the uniaxial magnetic anisotropy constant $K_u = 10^6 - 10^7$ J m^{-3} and moderate saturation magnetization $M_s = 11.25 \times 10^5$ A m^{-1} [48, 62–65]. Together with high corrosion resistance, these properties have already made FePt films applicable for the perpendicular magnetic recording media with the recording density exceeding 1 TBit/in^2 [66]. On the other hand, a very high coercivity, exceeding 10 T [67], and the corresponding high magnetic energy product provide new possibilities for the applications of FePt, such as microelectromechanical systems [68], ultra-strong permanent magnets [69] or FM-superconducting heterostructures [70].

We consider FePt thin film with the following parameters for incorporation with the Nb/AlO$_x$/Nb SIS junction: the thickness $d_F = 100$ nm $\simeq d_J$, the width $W = 1.5$ μm, equal to the LJJ width, the magneto-crystalline anisotropy $K_u = 5 \times 10^6$ J m^{-3}, the Gilbert damping $\alpha_F = 0.02$, the exchange constant $A = 10^{11}$ J m^{-1}. High K_u provides anisotropy field $H_a = 2K_u/\mu_0 M_s \simeq 7 \times 10^6$ A m^{-1} and natural resonance frequency $f_{FMR} = 207$ GHz, according to the Kittel formula $f_{FMR} = \gamma_0/2\pi (H - M_s + H_a)$, valid for a thin film with out-of-plane easy magnetization axis in out-of-plane magnetic field H [71]. The sub-THz FMR frequency of FePt was confirmed recently using so-called optical FMR [72]. The resonant length of this LJJ/FM hybrid is $L_{res} = \bar{c}/2f_{FMR} = 21.5$ μm. For calculations the FM layer is meshed with $\Delta x_F \times \Delta y_F \times \Delta z_F = 0.2 \times 0.5 \times d_F$ μm^3 cells and the finite difference $\Delta_J = \Delta y_F$ is used for the LJJ.
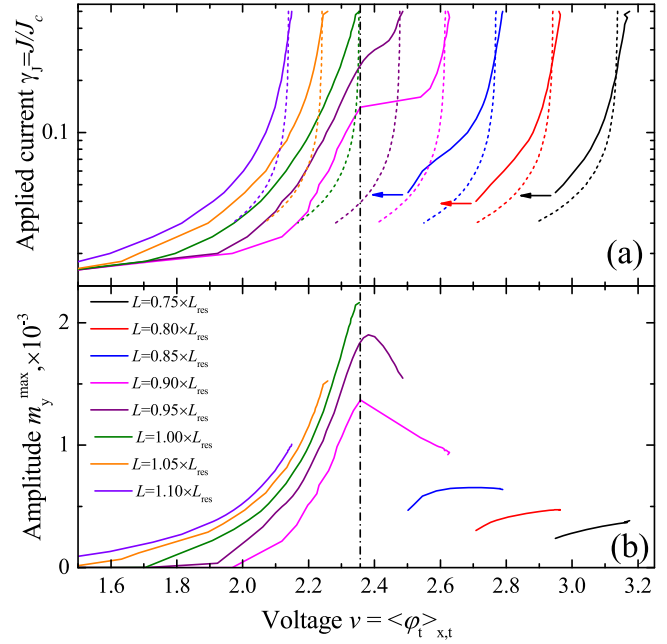

Figure 2. Coupling of the soliton with the FM at the fundamental harmonic. (a) Current–voltage characteristics in reduced units for Nb/AlO$_x$/Nb LJJ coupled to $L1_0$-FePt layer. Dashed lines of corresponding color indicate asymptotic *I–V* characteristics of LJJ with no FM according to equation (5). Dash–dot line indicates voltage where $f_J = f_{FMR}$. (b) Amplitude of magnetization precession in the FM layer.

Figure 2(a) shows *I–V* characteristics of devices of different length varied near the L_{res}. These current–voltage characteristics are reversible. Asymptotic *I–V*s for the LJJ in absence of the FM are also shown with dashed lines. Asymptotic *I–V* curves are calculated using the following unitless expression [73]

$$v = \frac{V}{\Phi_0} \frac{2\pi}{\omega_J} = 2\pi \frac{\bar{v}}{\bar{c}} \frac{\lambda_J}{L} = \frac{2\pi/l}{\sqrt{1 + (4\alpha_J/(\pi\gamma_J))^2}} \qquad (5)$$

with $l = L/\lambda_J$. The equation (5) also corresponds to the velocity of the soliton in LJJ $\bar{v} = v\bar{c}l/2\pi$ and is valid at $\gamma_J \gg \alpha_J$.

Simulations of the hybrid operation show that, in general, the coupling of the shuttling soliton to the FM induces a precession of the magnetic moment in the form of a synchronized magnetostatic standing wave of half wavelength ($\lambda_F/2$) with the nodes located at the edges of the device. The dependence of amplitudes of the standing wave on the recorded voltage ($m_y^{max}(v)$) are shown in figure 2(b). Simulations show a rigid dependence of the response on the length of the device as follows. For $L < 0.9L_{res}$ a coupling start to take place at high γ, and the AC soliton field produces precession of magnetization in FM of a finite amplitude. Interaction of the soliton with the FM slows the soliton down and causes the deviation of the *I–V*s from the asymptotes. Upon decreasing the current the soliton widens. At $\gamma \simeq 0.04$ the size of the soliton solution becomes comparable with the length of LJJ L, and the ZFS mode is no longer maintained (the transition to the zero voltage mode is indicated by the
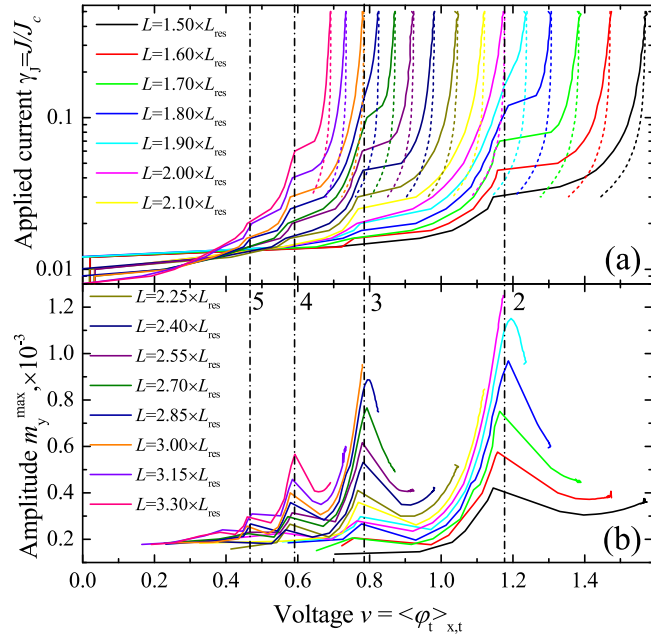
Figure 3. Coupling of the soliton with the FM at higher harmonics. (a) Current–voltage characteristics in reduced units for Nb/AlO$_x$/Nb LJJ coupled to $L1_0$-FePt layer. Dashed lines of corresponding color indicate asymptotic I–V characteristics of LJJ with no FM according to equation (5). Dash–dot lines with number n indicate voltage where $nf_J = f_{FMR}$. (b) Amplitude of magnetization precession in the FM layer.

Figure 4. Snapshots of magnetostatic standing waves $m_y(x)$ in $L1_0$-FePt FM layer at resonant coupling with Nb/AlO$_x$/Nb LJJ.

arrows in figure 2(a)). The resonant synchronization does not occur for these lengths since at $f_J = f_{FMR}$ the ZFS mode is not maintained. For $L = 0.9L_{res}$ and $L = 0.95L_{res}$ values of f_{ZFS} and f_{FMR} are closer and resonant synchronization emerges indicated by additional constant voltage step on I–Vs at $v = 2.35$ and corresponding maximum of $m_y^{max}(v)$. Since the additional step manifests the FMR, the voltage V of the step corresponds directly to the frequency of the FMR as $f_{FMR} = V/2\Phi_0$. Step features on I–V curves remind Fiske steps, originated from coupling of fluxons with a plasma wave that they generate during their propagation. Origin of steps in LJJ/FM hybrid is phenomenologically similar and results from coupling of propagating soliton with resonating magnetostatic wave that it generates. We emphasize that the coupling mechanism in the hybrid is essentially similar to one discussed for soliton dynamics in circular junction in external magnetic field [41–46]. For $L > L_{res}$ synchronization also takes place and the precessing magnetization provides additional strong damping visible as a deviation from I–V asymptotes. However, resonant synchronization does not occur and resonant steps are not observed since $f_{ZFS} < f_{FMR}$.

Figure 2 illustrates a coupling the soliton to the FM at the fundamental harmonic, i.e., at $f_J = f_{FMR}$. Since the soliton AC magnetic field is periodic and nonsinusoidal, the coupling with higher nth harmonics is also expected, i.e. at $nf_J = f_{FMR}$. In order to explore it, the length of the device should be increased. Figure 3(a) shows I–V characteristics of the device of different length L varied from $1.5L_{res}$ to $3.3L_{res}$. Except for the $L = 1.5L_{res}$ all the I–Vs (figure 3(a)) and $m_y^{max}(v)$ (figure 3(b)) curves continuously indicate two resonant modes: the one at

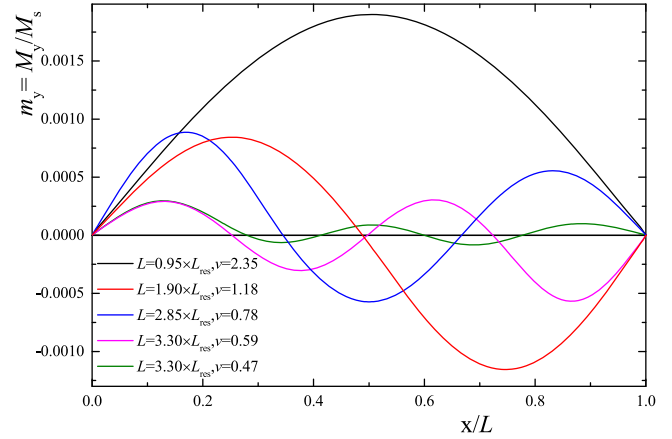$f_{FMR} = nf_J$ and the following one at $f_{FMR} = (n + 1)f_J$. From $n = 2$ up to $n = 5$ modes are observed. At that, the wavelength of magnetostatic standing wave also corresponds to the harmonic, i.e., $n\lambda_F/2 = L$. This result is of particular importance, since it denotes that exact matching of LJJ length to L_{res} is not necessary, the resonant synchronization will securely be observed for any $L > 1.5L_{res}$.

The physics shown in figures 2 and 3 is quite easy to interpret using both energy and dynamic consideration. Energy consideration imply absorption of LJJ energy $\sim IV$ by the FM at FMR. Dynamic considerations imply deceleration of the soliton propagation due to continuous experience of the attraction to the closest antinode position of the synchronized magnetostatic standing wave. A snapshots of magnetostatic standing waves $m_y(x)$ of maximum amplitude for each mode n observed in figures 2 and 3 are demonstrated in figure 4.

It is worth to estimate magnetostatic fields which provide the coupling. The soliton field can be simply estimated as $H^J \sim \Phi_0/(\lambda_J\lambda_L) \approx 50$ Oe. The y-component of magnetostatic field produced by the FM is $H_y^F \lesssim m_{max}^y N_y M_s \approx 1.5$ Oe, where $m_{max}^y \simeq 2 \times 10^{-3}$ (figure 4), N_y is an y-component demagnetizing factor [74, 75]. The zero-field mode is maintained since $H^F \ll H^J$.

3.2. SIS LJJ with low Swichard velocity coupled to the FM with in-plane anisotropy

Now we consider a different FM with high natural FMR frequency and strong *in-plane* magnetic anisotropy (i.e., magnetization $\vec{m}$ is aligned along x-direction in figure 1), and select a LJJ with appropriate properties for resonant coupling. One of the highest natural $f_{FMR} \sim 10$ GHz for FM with in-plane magnetic anisotropy was reported recently in [76], where a unique needle micro-structure of 40 nm thick CoFeB was obtained due to self-shadowing effect during film deposition at 70° of oblique angle. Resulting high value of natural f_{FMR} of CoFeB is justified by both high saturation magnetization $M_s = 14.75 \times 10^5$ A m^{-1} and anisotropy field $H_a = 4.85 \times 10^4$ A m^{-1}. Since the comfortable length of the device for both fabrication and numerical investigation ranges within ~ 10–100 μm, the LJJ should have an exceptionally

low Swihart velocity $\bar{c} = 2Lf_{\mathrm{FMR}} \sim 2 \times 10^5 - 10^6$ m s^{-1} to be coupled with CoFeB.

In general, the Swihart velocity $\bar{c} = \lambda_{\mathrm{J}}\omega_{\mathrm{J}} = \sqrt{t_{\mathrm{ox}}/\varepsilon_0\varepsilon\mu_0 d_{\mathrm{J}}}$ is determined by the thickness and the permittivity of the tunnel barrier, as well as by the magnetic thickness. LJJs based on NbO$_x$ with $\varepsilon \sim 40$ can be considered since its permittivity $\varepsilon \sim 40$ reduces $\bar{c}$ by factor of 2 as compared to AlO$_x$ based junctions of the same geometry and magnetic thickness. Quite a number of works is available on Nb/NbO$_x$/Nb and Nb/NbO$_x$/Pb junctions (see for example [77, 78] and [79, 80], respectively). Yet, in these works junctions with high $\bar{c} \sim 10^7$ m s^{-1} are reported probably due to technologically limited large thickness t_{ox} of the barrier. On the other hand $\bar{c}$ is reduced significantly for the LJJ with thin tunnel barrier t_{ox} and/or for the LJJ with electrodes of large λ_L. Our attention was drawn to [81] where authors have reported fabrication of the MgB$_2$/AlN/NbN Josephson tunnel junction. Sub-nm thickness of the tunnel barrier $t_{\mathrm{ox}} \sim 0.14$ nm and large average London penetration depth of the electrodes $\lambda_{\mathrm{L}} = (\lambda_{\mathrm{L}}(\mathrm{MgB}_2) + \lambda_{\mathrm{L}}(\mathrm{NbN}))/2$–100 nm provide the $\bar{c} \simeq 2 \times 10^6$ m s^{-1}.

Therefore, we consider MgB$_2$/AlN/NbN SIS junction with the following properties [81] to be coupled to the CoFeB FM: the critical current density $J_{\mathrm{c}} = 1 \times 10^7$ A m^{-1}, the permittivity of AlN tunnel barrier $\varepsilon \simeq 10$, the thickness of the barrier $t_{\mathrm{ox}} \simeq 0.14$ nm, average London penetration depth $\lambda_{\mathrm{L}} \simeq 10^{-7}$ m, the dissipation coefficient $\alpha_{\mathrm{J}} = 0.01$, the surface loss parameter $\beta = 0.002 \ll \alpha_{\mathrm{J}}$. These parameters provide the Josephson penetration depth $\lambda_{\mathrm{J}} \simeq 11.4$ μm, the Josephson frequency $\omega_{\mathrm{J}} \simeq 2.19 \times 10^{11}$ Hz, and the Swihart velocity $\bar{c} = 2.5 \times 10^6$ m s^{-1}. Low $\bar{c}$ is justified by the reduced ω_{J}.

For successful coupling several following issues need to be addressed. According to the Kittel formula for in-plane geometry [48] $f_{\mathrm{FMR}} = \gamma_0/2\pi\sqrt{(H + H_a + M_s)(H + H_a)}$. Natural FMR frequency of 10 GHz requires the resonant length $L_{\mathrm{res}} = \bar{c}/2f_{\mathrm{FMR}} \sim 100$ μm. However, for accurate derivation of the natural FMR we also need to take into account the effective field of shape anisotropy. The shape anisotropy of a bar-shaped FM of length L, width W and thickness d_F [74, 75, 82, 83] provides additional anisotropy field $H_{\mathrm{SA}}/M_s \simeq d_F(\sqrt{4L^2 + W^2} - W)/(\pi LW) = 0.017$, which is comparable with the growth induced anisotropy field $H_a/M_s = 0.033$. Also we should note that our original attempts for LJJ/FM simulation failed. Strong coupling and in-plane geometry enables high amplitude of magnetization precession ($m_y^{\mathrm{max}} M_s$) and consequently strong magnetostatic field H_y^F in the LJJ, which breaks the ZFS mode. Therefore we have to suppress the inductive coupling. In order to keep computational integrity we consider a nonmagnetic layer of thickness d_n distributed above and below the FM as shown in figure 5. The nonmagnetic layer allows the magnetic flux of the soliton to be redistributed and the magnetic field in FM to be reduced accordingly ($H^J d_{\mathrm{J}}/(d_F + d_d)$). Smaller AC field induces precession of magnetic moment in FM with lower m_y^{max} and consequently reduces the magnetostatic field H_y^F in LJJ. We found that $d_d = 5d_F = 200$ nm is sufficient to maintain the ZFS mode. Finally we apply small magnetic field along the device to compensate the negative stray field H_x^F/M_s produced by the magnetized FM in the LJJ. The
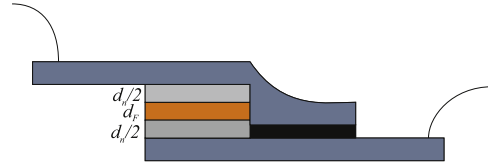

Figure 5. A schematic crossection of the hybrid device with in-plane magnetization orientation and reduced inductive coupling. Ferromagnetic layer of thickness d_F (shown in orange) is placed between two nonmagnetic layers of total thickness d_n and in close proximity to the Josephson tunnel layer (shown in black).
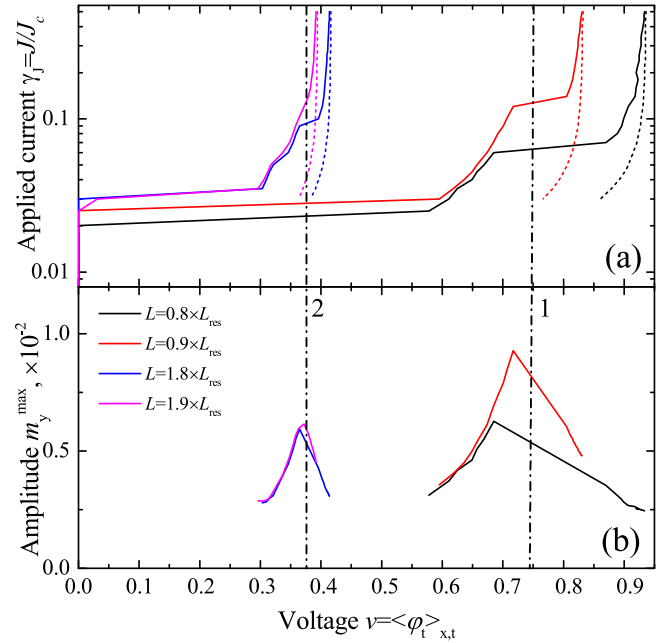

Figure 6. Coupling of the soliton with the FM. (a) Current–voltage characteristics in reduced units for MgB$_2$/AlN/NbN LJJ coupled to CoFeB layer. Dashed lines of corresponding color indicate asymptotic I–V characteristics of LJJ with no FM according to equation (5). Dash–dot lines with number n indicate voltage where $nf_{\mathrm{J}} = f_{\mathrm{FMR}}$. (b) Amplitude of magnetization precession in the FM layer.

typical compensating applied magnetic field $h = -H_x^F/M_s \lesssim 0.002$. All field contributions (H_{SA}, H_a and H_x^F) provide the FMR frequency $f_{\mathrm{FMR}} \simeq 13$ GHz and the resonant length $L_{\mathrm{res}} = \bar{c}/2f_{\mathrm{FMR}} \simeq 96$ μm. For calculations the FM layer is meshed with $\Delta x_F \times \Delta y_F \times \Delta z_F = 0.4 \times 0.5 \times d_F$ μm^3 cells and the finite difference $\Delta_J = \Delta y_F$ is used for the LJJ.

Figure 6 shows I–V and $m_y^{\mathrm{max}}(v)$ characteristics of hybrid devices of several selected lengths. Asymptotic I–Vs for LJJ in absence of the FM (equation (5)) are also shown with dashed lines. A snapshots of magnetostatic standing waves $m_y(x)$ distribution of maximum amplitude for each mode observed are demonstrated in figure 7.

Qualitatively, the behavior of CoFeB-based LJJ/FM repeats one of FePt-based LJJ/FM device. The major difference is by the order of magnitude higher amplitude of magnetization precession m_y^{max} of CoFeB, despite the reduction of coupling by thick nonmagnetic layer. Large amplitude
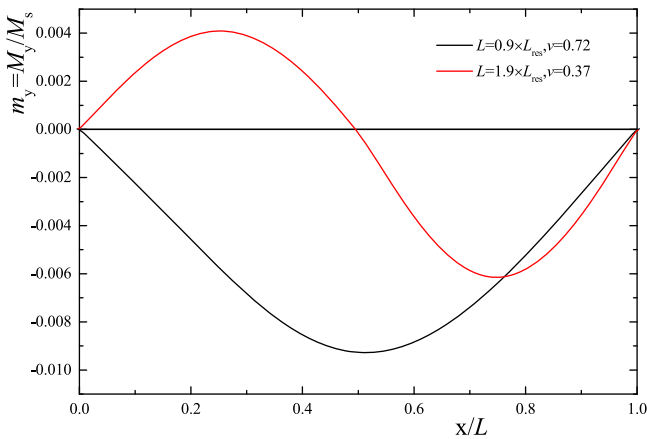
Figure 7. Snapshots of magnetostatic standing waves $m_y(x)$ in CoFeB FM layer at resonant coupling with $MgB_2/AlN/NbN$ LJJ.

m_y^{max} is justified by the in-plane magnetization and weaker anisotropy energy. The soliton field provided by the $MgB_2/AlN/NbN$ LJJ is $H^J \approx 15$ Oe, while the y-component of magnetostatic field produced by the CoFeB is $H_y^F \lesssim 3$ Oe, according to figure 7. Hence, the ZFS mode was not maintained originally since H^J and H_y^F are comparable in absence of nonmagnetic layer.

4. Summary

Summarizing, in this work, we propose a hybrid system of long JJ coupled to an external magnetic layer with the following operation principle. The soliton in LJJ in zero-field mode synchronizes with magnetostatic standing wave of FM that it generates. The synchronization damps additionally the soliton motion providing a deviation of I–V characteristics from the asymptotic one in accordance with Gilbert damping. Fiske-like additional constant voltage steps on the ZFS I–V characteristics appear at voltages where resonant synchronization takes place and the frequency of soliton AC field f_J matches the FMR frequency.

We see a potential for application of the proposed device at least in two possible ways. First, it allows to measure the FMR frequency of individual micrometer-scaled FM samples with high intrinsic magnetic anisotropy employing just DC technique. In particular, natural FMR of FePt can hardly be measured using a conventional vector-network-analyzer (VNA) approach since the frequency of typical commercially available VNA is limited by several tens of GHz. Second, multiple LJJs of varied geometry and/or Josephson properties can all be synchronized to an operation frequency determined by the FM characteristics of common FM layer or identical FMs, including shape of FM.

We emphasize that the proposed hybrid device can be fabricated considering a variety of realistic FM materials and superconducting JJs.

References

[1] Clarke J and Braginski A I 2005 *The SQUID Handbook* vol 1 (Weinheim: Wiley-VCH)
[2] Weinstock H 1996 *SQUID Sensors: Fundamentals, Fabrication and Applications* (Dordrecht: Springer Science + Business Media)
[3] Granata C and Vettoliere A 2016 *Phys. Rep.* **614** 1
[4] Brock D K, Track E K and Rowell J M 2000 *IEEE Spectr.* **37** 40
[5] Holmes D S, Ripple A L and Manheimer M A 2013 *IEEE Trans. Appl. Supercond.* **23** 1701610
[6] Kirichenko D E, Sarwana S and Kirichenko A F 2011 *IEEE Trans. Appl. Supercond.* **21** 776
[7] Vernik I V, Kaplan S B, Volkmann M H, Dotsenko A V, Fourie C J and Mukhanov O A 2014 *Supercond. Sci. Technol.* **27** 044030
[8] Volkmann M H, Vernik I V and Mukhanov O A 2015 *IEEE Trans. Appl. Supercond.* **25** 1301005
[9] Herr Q P, Herr A Y, Oberg O T and Ioannedis A G 2011 *J. Appl. Phys.* **109** 103903
[10] Feofanov A K et al 2010 *Nat. Phys.* **6** 593
[11] Bakurskiy S V, Klenov N N, Soloviev I I, Bol'ginov V V, Ryazanov V V, Vernik I V, Mukhanov O A, Kupriyanov M and Golubov A A 2013 *Appl. Phys. Lett.* **102** 192603
[12] Larkin T I, Bol'ginov V V, Stolyarov V S, Ryazanov V V, Vernik I V, Tolpygo S K and Mukhanov O A 2012 *Appl. Phys. Lett.* **100** 222601
[13] Gingrich E C et al 2016 *Nat. Phys.* **12** 564
[14] Linder J and Robinson J W A 2015 *Nat. Phys.* **11** 307
[15] Buzdin A I 2005 *Rev. Mod. Phys.* **77** 935
[16] Jung P, Butz S, Marthaler M, Fistul M V, Leppäkangas J, Koshelets V P and Ustinov A V 2014 *Nat. Commun.* **5** 3730
[17] Jung P, Butz S, Shitov S V and Ustinov A V 2013 *Appl. Phys. Lett.* **102** 062601
[18] Zhang D, Trepanier M, Mukhanov O and Anlage S M 2015 *Phys. Rev. X* **5** 041045
[19] Ustinov A V 2015 *IEEE Trans. Terahertz Sci. Technol.* **5** 1
[20] Clarke J and Wilhelm F K 2008 *Nature* **453** 1031
[21] Erné S N, Ferrigno A and Parmentier R D 1983 *Phys. Rev. B* **27** 5440
[22] Cirillo M, Grønbech-Jensen N, Samuelsen M R, Salerno M and Rinati G V 1998 *Phys. Rev. B* **58** 12377
[23] Jaworski M 1999 *Phys. Rev. B* **60** 7484
[24] Nagatsuma T, Enpuku K, Irie F and Yoshida K 1983 *J. Appl. Phys.* **54** 3302
[25] Koshelets V, Shchukin A, Shitov S and Filippenko L 1993 *IEEE Trans. Appl. Supercond.* **3** 2524

[26] Mygind J, Koshelets V, Shchukin A, Shitov S and Lapytskaya I 1995 *IEEE Trans. Appl. Supercond.* **5** 2951
[27] Pankratov A L, Fedorov K G, Salerno M, Shitov S V and Ustinov A V 2015 *Phys. Rev.* B **92** 104501
[28] Davidson A, Pedersen N F and Pagano S 1986 *Appl. Phys. Lett.* **48** 1306
[29] Lachenmann S G *et al* 1995 *J. Appl. Phys.* **77** 2598
[30] Lomdahl P S, Soerensen O H and Christiansen P L 1982 *Phys. Scr.* **25** 879
[31] Lomdahl P S, Soerensen O H and Christiansen P L 1982 *Phys. Rev.* B **25** 5737
[32] Barbara P, Monaco R and Ustinov A V 1996 *J. Appl. Phys.* **79** 327
[33] Scheuermann M, Chen J T and Chang J J 1983 *J. Appl. Phys.* **54** 3286
[34] Maksimov A G, Nekorkin V I and Rabinovich M I 1995 *Int. J. Bifurcation Chaos* **5** 491
[35] Pedersen N F and Davidson A 1990 *Phys. Rev.* B **41** 178
[36] Cirillo M and Lloyd F L 1987 *J. Appl. Phys.* **61** 2581
[37] Ustinov A *et al* 1996 *Phys. Rev.* B **54** 6111
[38] Parmentier R D *et al* 1997 *Phys. Rev.* B **55** 15165
[39] Holst T, Hansen J B, Grnbech-Jensen N and Blackburn J A 1990 *Phys. Rev.* B **42** 127
[40] Sakai S, Bodin P and Pedersen N F 1993 *J. Appl. Phys.* **73** 2411
[41] Martucciello N and Monaco R 1996 *Phys. Rev.* B **53** 3471
[42] Wallraff A *et al* 2000 *J. Low Temp. Phys.* **118** 543
[43] Vernik I V *et al* 1997 *J. Appl. Phys.* **81** 1335
[44] Gronbech-Jensen N, Lomdahl P S and Samuelsen M R 1991 *Phys. Lett.* A **154** 14
[45] Gronbech-Jensen N 1992 *Phys. Rev.* B **45** 7315
[46] Gronbech-Jensen N *et al* 1992 *Phys. Rev.* B **46** 294
[47] Kittel C 1948 *Phys. Rev.* **73** 155
[48] Àlvarez N, Alejandro G, Gòmeza J, Goovaerts E and Butera A 2013 *J. Phys. D: Appl. Phys.* **46** 505001
[49] Monaco R, Cristiano R, Frunzio L and Nappi C 1992 *J. Appl. Phys.* **71** 1888
[50] Imamura T, Shiota T and Hasuo S 1992 *IEEE Trans. Appl. Supercond.* **2** 1
[51] Imamura T, Shiota T and Hasuo S 1992 *IEEE Trans. Appl. Supercond.* **2** 84
[52] Shiota T, Imamura T and Hasuo S 1992 *IEEE Trans. Appl. Supercond.* **2** 222
[53] Miller R E, Mallison W H, Kleinsasser A W, Delin K A and Macedo E M 1993 *Appl. Phys. Lett.* **63** 1423
[54] Kaiser C, Meckbach J M, Ilin K S, Lisenfeld J, Schäfer R, Ustinov A V and Siegel M 2011 *Supercond. Sci. Technol.* **24** 035005
[55] Meckbach J M, Merker M, Buehler S J, Ilin K, Neumeier B, Kienzle U, Goldobin E, Kleiner R, Koelle D and Siegel M 2013 *IEEE Trans. Appl. Supercond.* **23** 1100504
[56] Barone A and Paterno G 2005 Fluxon dynamics *Physics and Applications of the Josephson Effect* (New York: Wiley) ch 10
[57] Soriano C, Costabile G and Parmentier R D 1996 *Supercond. Sci. Technol.* **9** 578
[58] Ustinov A V 1998 *Physica* D **123** 315
[59] Gronbech-Jensen N *et al* 1991 *Phys. Rev.* B **43** 12799
[60] Miltat J E and Donahue M J 2007 Numerical micromagnetics: finite difference methods *Handbook of Magnetism and Advanced Magnetic Materials* vol 2 (New York: Wiley)
[61] Nakatani Y, Uesaka Y and Hayashi N 1989 *J. Appl. Phys.* **28** 2485
[62] Okamoto S, Kikuchi N, Kitakami O, Miyazaki T, Shimada Y and Fukamichi K 2002 *Phys. Rev.* B **66** 024413
[63] Iihama S, Sakuma A, Naganuma H, Oogane M, Miyazaki T, Mizukami S and Ando Y 2014 *Appl. Phys. Lett.* **105** 142403
[64] Golovchanskiy I A, Fedoseev S A and Pan A V 2013 *J. Phys. D: Appl. Phys.* **46** 215502
[65] Ho P, Evans R F L, Chantrell R W, Han G, Chow G M and Chen J 2015 *J. Appl. Phys.* **117** 213901
[66] Kryder M H *et al* 2008 *Proc. IEEE* **96** 1811
[67] Shima T *et al* 2004 *Appl. Phys. Lett.* **85** 2571
[68] Fähler S *et al* 2004 *Proc. 18th Intl. Workshop on High Performance Magnets and their Applications* 2(*Annecy, France*) 566
[69] Bader S D 2006 *Rev. Mod. Phys.* **78** 1
[70] Haindl S *et al* 2008 *Supercond. Sci. Technol.* **21** 045017
[71] Beaujour J M, Ravelosona D, Tudosa I, Fullerton E E and Kent A D 2009 *Phys. Rev.* B **80** 180415R
[72] Becker J, Mosendz O, Weller D, Kirilyuk A, Maan J C, Christianen P C M, Rasing T and Kimel A 2014 *Appl. Phys. Lett.* **104** 152412
[73] McLaughlin D W and Scott A C 1978 *Phys. Rev.* A **18** 1652
[74] Aharoni A, Pust L and Kief M 2000 *J. Appl. Phys.* **87** 6564
[75] Aharoni A 1998 *J. Appl. Phys.* **83** 3432
[76] Li C, Chai G, Yang C, Wang W and Xue D 2015 *Sci. Rep.* **5** 17023
[77] Hawkins G and Clarke J 1976 *J. Appl. Phys.* **47** 1616
[78] Aponte J, Rivera E, Neto A S and Octavio M 1987 *J. Appl. Phys.* **62** 700
[79] Karulkar P C and Nordman J E 1979 *J. Appl. Phys.* **50** 7051
[80] Dueholm B, Levring O A, Mygind J, Pedersen N F and Soerensen O H 1981 *Phys. Rev. Lett.* **46** 1299
[81] Shimakage H, Tsujimoto K, Wang Z and Tonouchi M 2004 *Supercond. Sci. Technol.* **17** 1376
[82] Li Y, Lu Y and Bailey W E 2013 *J. Appl. Phys.* **113** 17B506
[83] Vroubel M, Zhuang Y, Rejaei B, Burghartz J N, Crawford A M and Wang S X 2004 *IEEE Trans. Mag.* **40** 2835